AUTOMATIC 3D-LOCALISATION OF BURIED PIPELINE AND DEPTH OF COVER: Magnetic investigation under operational conditions

Mehdi M. LAICHOUBI[1], M. Eng ; Marc MUNSCHY[2], PhD ; Samir TAKILLAH[1], PhD ;
Sylvain DECOMBE[1], M. Eng ; Vincent BENET[1], M. Eng ;
Aude LABROSSE[3] ; Damien LEFEBVRE[3]

1- **Skipper NDT**, R&D Department, Paris, France.
2- **Institut Terre et Environnement de Strasbourg**, UMR 7063, Université de Strasbourg/EOST, CNRS, Strasbourg, France.
3- **Teréga**, Pipeline Inspection Department; Pau, France.

Keywords: Magnetic Inverse Problem, Magnetic Map, Fluxgate Magnetometer, Geographic Information System, Depth of Cover, Non-Destructive Testing.

ABSTRACT

Pipeline operators need to 3D-geolocalize their buried pipelines for two main reasons: to update their network's Geographic Information System and for safety considerations, in particular to determine the depth of cover. The latter is a key parameter to ensure the network's protection in case of third-party interferences. Several methods are available for pipeline geolocalization, such as electromagnetism, in particular, radio-frequency techniques and ground-penetrating radar. They all entail either specific soil conditions or are manual (prone to human error) and time-consuming.

Skipper NDT has developed a proprietary method to provide precise and continuous coordinates (longitude, latitude) and depth of cover of buried pipelines, using large standoff magnetometry (LSM). The patented hardware measures the magnetic field above the pipeline, using fluxgate three-component magnetometers and a GNSS. To determine a precise position, an algorithm performs 2D and 3D magnetic data inversions along the magnetic map for automatic detection and georeferencing. Performances of Skipper NDT's detections were tested under field conditions and compared to land surveyor's results, thanks to a collaboration with the French gas operator Teréga. Compared to the 3D reference, the accuracy is at least 0.2 m for 90% of measured data.

I. INTRODUCTION

3D localization of pipelines uses different technologies, one of the most commonly employed being based on electromagnetic theory [1]-[2]. This technique needs the pipeline to be conductive and an alternating current must be injected. The resulting magnetic field radiated by the pipeline is measured by a handheld receiver [3]-[4]-[5]. Other techniques more or less employed are ground penetrating radar, infrared thermography and acoustic localization [1]. There is not much work showing results obtained with magnetic mapping also called magnetic tomographic method (MTM) or large standoff magnetometry (LSM). MTM/LSM is generally used to detect changes in the magnetic field of a pipeline due to changes in the steel magnetization. These changes are often interpreted in relation with magnetostriction (e.g. the Villari effect) [6]. However, the magnetic map is rarely used to define the horizontal location and its depth below the ground. Vo et al. [7], propose an inversion method to determine the depth and location of buried pipes using the magnetic field components values along the

pipeline. Li et al. [8] develop a method based on a combination of tilt angle and downward computation of the magnetic field intensity map.

In the present study, we present the method used by Skipper NDT to perform the magnetic survey using a ground-based mobile equipment, then describe the principles of the method used to determine the depth and location of buried pipes and finally show results obtained using magnetic data acquired above a pipe.

II. MAGNETIC MAPPING PROTOCOL

In terms of hardware, the Skipper NDT team has patented a ground-based mobile equipment that can be pulled by an operator or towed by a vehicle (Figure 1). The main components of the device are: 1) 5 three-components fluxgate magnetometers; 2) a real-time GNSS/RTK navigation system with a centimetric precision; 3) a Tactical grade Inertial Measurement Unit (IMU) and 4) a proprietary electronic card for data acquisition and integration. Data collection is also done using an Unmanned Aerial Vehicle with the same embedded devices (Figure 2). It allows an increasing productivity while enhancing field operators' safety.

Figure 1: SKIPPER NDT ground-based mobile equipment. A) geometric description. B) picture of the equipment during a field survey

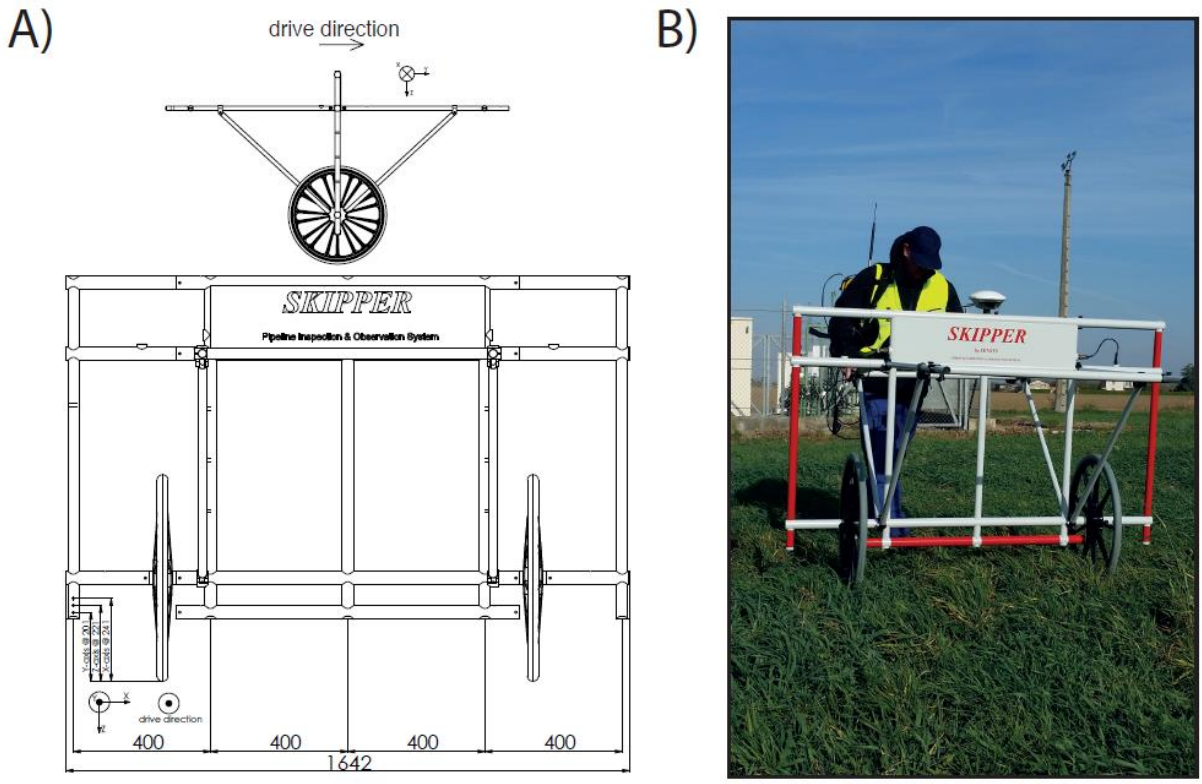

Figure 2. Off the shelf UAV with Skipper NDT's embedded system including: 5 three-components fluxgate magnetometers, a real-time GNSS/RTK navigation system with a centimetric precision, IMU and a proprietary electronic card for data acquisition and integration.

The main reasons for using three-components fluxgate magnetometers instead of scalar magnetometers is that measuring the components of the magnetic field allows to perform a compensation of the magnetic effect of the equipment. This subject is not new and has been developed in years 1970 to allow magnetic compensation of airplanes in airborne geophysics [9-10]. On the other hand, fluxgate magnetometers are not absolute, which is their main default. Thus, they must be calibrated. An easy to perform calibration procedure was proposed by [11]. It allows to compute the nine values of the sensor's defaults by only measuring the three components of the magnetic field at a given location and without the need to know the orientation of the sensor. This calibration method is referred to as scalar calibration [11]. Munschy et al. [12] have shown that both methods use the same kind of functions and that when calibration is performed, compensation also applies and reciprocally. Thus, before and after all surveys, a calibration procedure is performed: the frame is maintained above a mark on the ground and the operator turns the frame around this mark and changes its pitch at the same time. The duration of the operation is about one minute and after calibration the standard deviation of the calibrated magnetic field is about 1 nT (Figure 3).

Figure 3. Results of a calibration for one of the five magnetic sensors. A) the two curves correspond to the noncalibrated (blue line, standard deviation 85.1 nT) and calibrated (red line, standard deviation 1.7 nT) intensities of the magnetic field measured by the fluxgate sensor. The green curve is the intensity of the Earth's magnetic field at the location of the calibration. B) the nine estimated calibration parameters and their standard deviations.

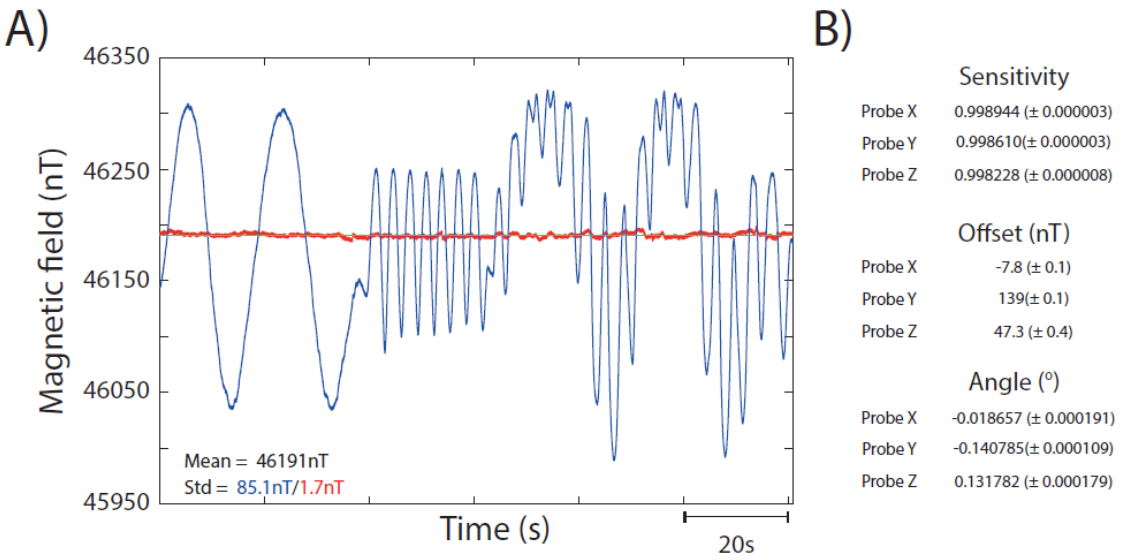

Parallel magnetic profiles are acquired above the buried pipeline and data is processed as follows to obtain the total magnetic intensity map: 1) use of calibration parameters to calibrate the data; 2) identify the beginning and end of each profile; 3) edit data to check for spikes; 4) compute the total magnetic intensity map by interpolation of data profiles. More often the node spacing of the magnetic map is 0.1 m. The total magnetic intensity map is then used to locate the pipeline by computing its horizontal location and depth below the ground.

III. THEORY OF 2D AND 3 D LOCALIZATION OF A BURIED PIPE

A Pipeline is formed of pipe sections welded together. The length of the sections varies generally between 5 and 15 m. Depending the depth below the ground and the length of each section, the total magnetic intensity can be regarded as due to an infinite horizontal cylinder or a sphere corresponding to the location of the weld. More often, due to the welding process and because the magnetization of each consecutive section is not the same, the amplitude of the magnetic anomaly at the section limits is greater than the amplitude on the rest of the section (Figure 4A). Geophysical interpretation uses total magnetic intensity maps or profiles to constrain the sources of magnetization generating the anomalies. There are many methods and tools to perform these interpretations, but the main difficulty is that, generally, a magnetic

anomaly can be caused by an infinite variety of sources, thus demonstrating the nonuniqueness of causative magnetization distributions. In the case of a pipeline, the situation is simpler: the magnetized object can be regarded as a finite length cylinder for which the three spatial coordinates have to be computed relying on the magnetic map location. A classic interpretation tool used in such a case is the analytic signal.

The application of analytic signal theory to 2D magnetic interpretation was proposed by [13]. Using the total magnetic intensity data (F) along a profile (x), the analytic signal (S) can be computed using

$$S(x) = \frac{\partial F(x)}{\partial x} - i\frac{\partial F(x)}{\partial z}$$

With $i^2 = -1$ and $\frac{\partial F(x)}{\partial z}$ the vertical derivative of F which is Hilbert Transform of the horizontal derivative of F. In geophysical interpretation, only the amplitude of the analytic signal is used and Nabighian et al. [13] have shown that the amplitude of the analytic signal due to a finite magnetized step is a bell-shaped function. Its maximum is at the horizontal location of the step, and has the property of having its half-maximum, at the half-width, equal to the depth of the step. The shape of the analytic signal does not depend on the direction of the Earth's magnetic field nor on the direction of magnetization nor the profile. Only its amplitude varies according to the angles of the latter three vectors. For a cylinder located at $(x_{0,}z_0)$, the same properties apply [14] and the analytic signal is equal to

$$S(x) = \frac{2C}{(x - i(z - z_0))^3}$$

with C a coefficient depending on the Earth's magnetic field direction, magnetization, and profile orientation [14].

The extension to three dimensions of the 2D analytic signal is more problematic because a complex function cannot be established using three partial derivatives [15]. However, the general formula used to define the 3D amplitude of the analytic signal corresponds to the definition of [16], i.e.

$$S(x,y) = \sqrt{\left(\frac{\partial F(x,y)}{\partial x}\right)^2 + \left(\frac{\partial F(x,y)}{\partial y}\right)^2 + \left(\frac{\partial F(x,y)}{\partial z}\right)^2}$$

and is called the "vector analytic signal". In our example, the vector analytic signal computed from the total magnetic intensity map of Figure 4A is displayed in Figure 4B. Using synthetic cases (e.g. [16]) the properties of the vector analytic signal have been established: a bell-shaped function with a maximum above the structure and a shape depending on the depth of the structure. However, [17] has shown that the shape of the vector analytic signal over a sphere source is dependent on the direction of magnetization and that the maximum horizontal shift can be up to 30% of the sphere depth.

IV. APPLICATION

Thanks to a collaboration with the French gas operator Teréga a field survey was performed in October 2019 along a 160 m long segment of a pipeline on their network. Its nominal diameter is 219 mm with an X42 steel grade. The pipeline was laid in 1965.

The magnetic map shown in Figure 4A was obtained using the field magnetic acquisition device described above. It results from the acquisition of five profiles spaced over 2 m with the five sensors 0,2 m above ground level. The map mainly shows the alignment of magnetic anomalies due to the pipe sections with an amplitude of about 4000 nT. The spatial derivatives of the magnetic map are computed and used to determine the analytic signal (Figure 4B).

Figure 4: A) total magnetic intensity map. Tracks of the mobile device are shown with black lines. B) analytic signal. Coordinates are in meters.

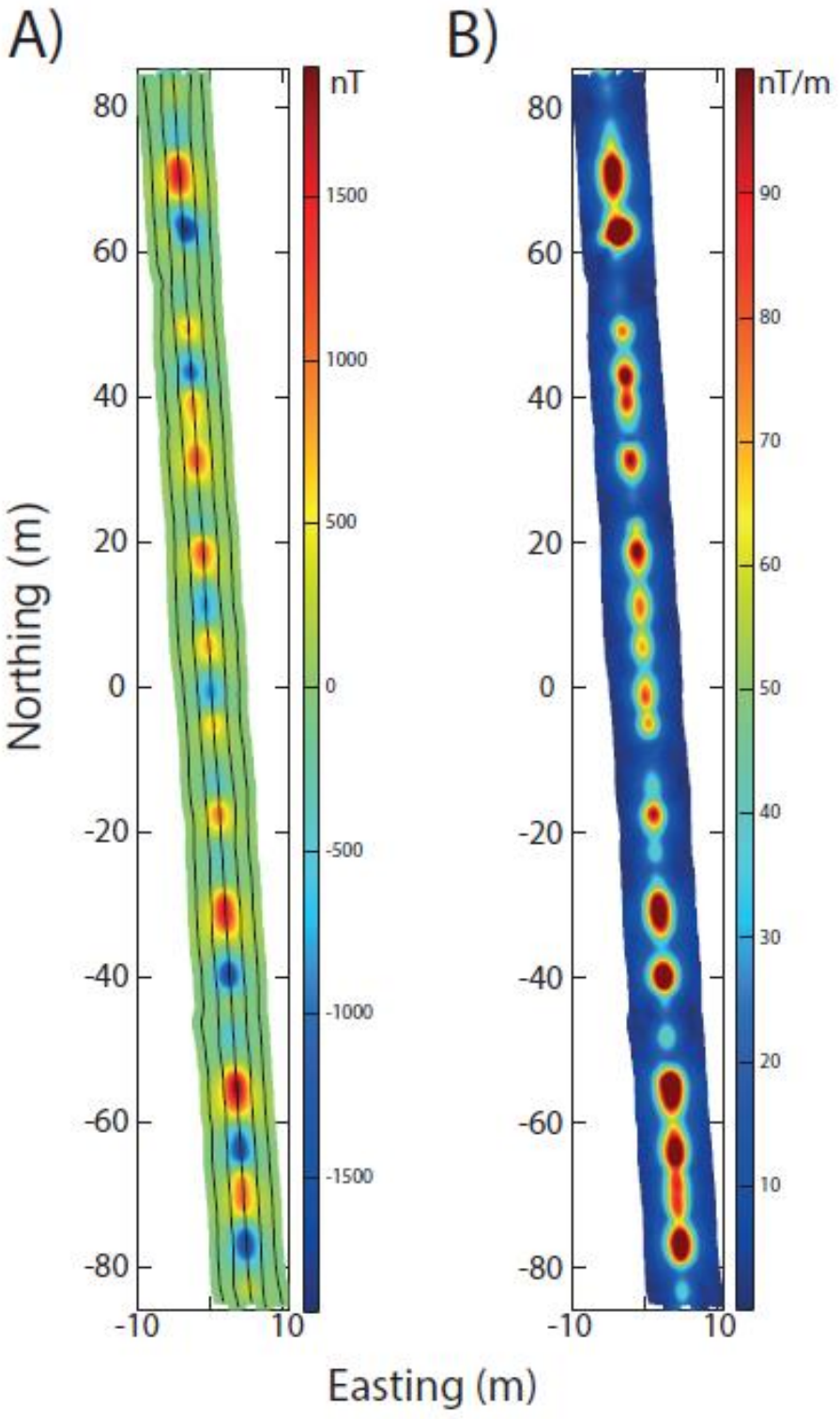

The two methods described above are used to compute the 3D location of the pipeline.

Profiles orthogonal to the pipeline direction are extracted from the analytic signal map (Figure 4B-5A) every 0.05 m and are used as an input to compute the horizontal and vertical location of the pipeline. The results are compared to the horizontal and vertical location obtained with the electromagnetic location [5] which serves as a reference. Figure 5B shows the horizontal difference: more often the difference is less than 0.05 m, but at some locations the difference is larger and can reach 0.3 m. For the vertical location, the differences compared to the electromagnetic method are larger, generally comprised between -0.2 and 0.2 m, but can reach values of more than 1 m (Figure 5C). Comparing with Figure 4A, the biggest differences are observed near limits of pipeline sections. To overcome this problem, a median of the depth values is computed along a sliding window of size 5 m. The resulting curve displayed in Figure 5C show a maximum difference of 0.36 m.

The performances of the 3D location of the pipeline using 2D inversion are summed up in Figure 6. The histograms compile the distance-errors to the reference line, presented in Figure 5B-C, along the pipeline. The results look like a folded normal distribution coherent with the fact that nonnegative distances are computed. The mean horizontal error is 0.08 m with a 0.05 m standard deviation and 90% of all given points fall under 0.14 m of error compared to the reference line. Concerning the depth below ground, the results show a mean error of 0.08 m, a 0.08 m standard deviation and 0.12 m 90^{th} percentile.

Using the analytic signal map (Figure 4B-5A), the local maxima of the grid are identified, and 3D inversion is applied in a window with a radius of 4 m. 22 maxima are found and the results obtained are shown by red circles in Figure 5B-C. The horizontal location obtained shows solid results with errors less than 0.05 m. For the depths of cover, the results are more problematic, with values ranging from 0.8 to 2.2 m. This is mainly due to the fact that the function used to perform the data inversion corresponds to the analytic signal of a sphere and not of a contact between to segments uniformly magnetized, with a possible demagnetized zone at the location of the contact.

Figure 5. Results of 2D and 3D analytic signal inversions. A) Analytic signal map. B) Horizontal location errors compared to the results of the electromagnetic handheld device [5]: the blue curve corresponds to the results of the 2D inversion and the red circles to the 3D inversion. C) Depths of cover obtained and compared to the electromagnetic handheld device results (black curve): the blue curve corresponds to the results of the 2D inversion and the red circles to the 3D inversion. The green curve corresponds to the application of the median of the blue curve along a 5-meter sliding window.

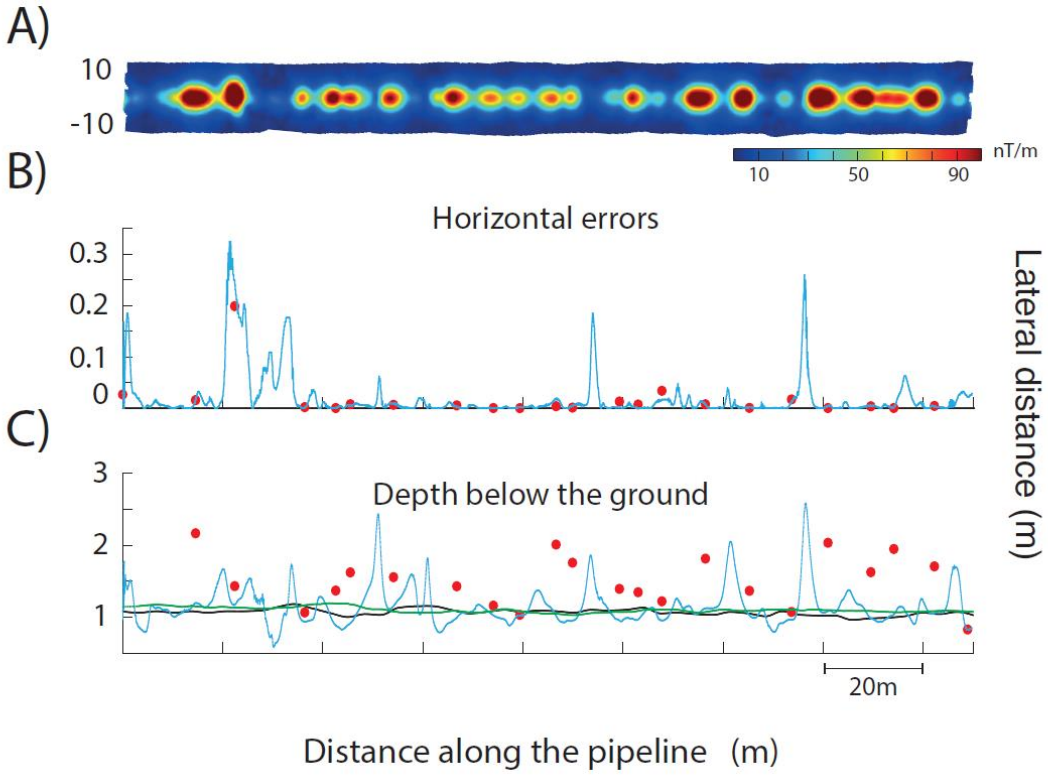

Figure 6. Histograms of distance-error of Skipper NDT's location to the reference line using 2D inversion. A) Histogram of horizontal errors to the reference line and its mean, standard deviation and 90th percentile. B) Depth of cover histogram errors to the reference line and its mean, standard deviation and 90th percentile.

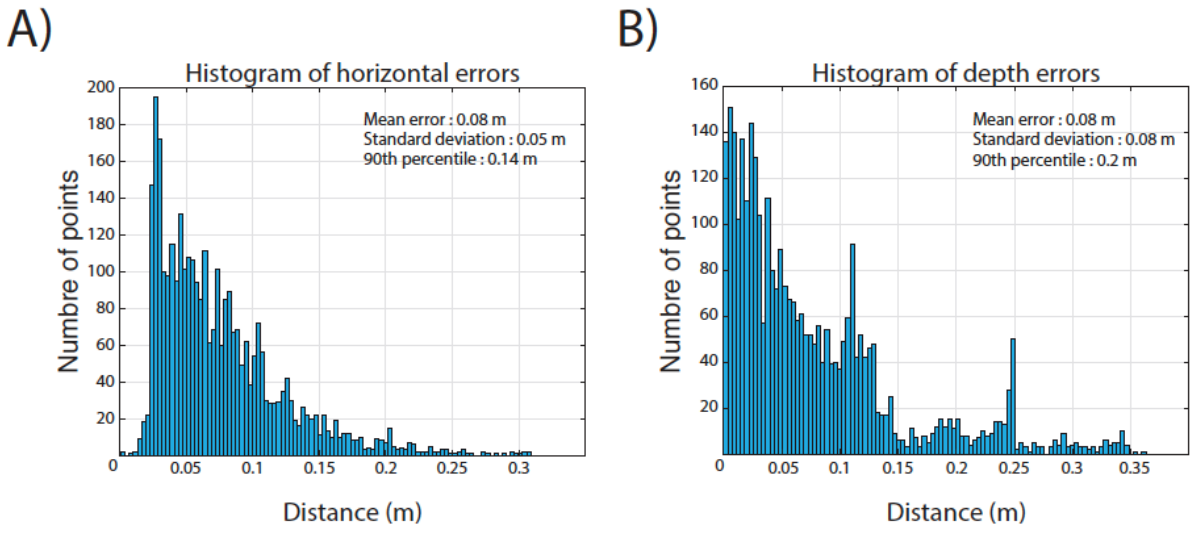

V. CONCLUSION

Magnetic mapping above pipeline is a rapid and efficient method which allows to obtain a magnetic anomaly map due to the magnetization of the pipeline. The magnetic map is used to compute the analytic signal map. The latter is used to perform 2D and 3D inversions. 2D inversion yields to good results compared to electromagnetic methods with differences less than 0.2 m in accuracy for 90% of measured data for both horizontal and depth positioning. Although 3D inversion results give good horizontal location, it is less the case for depth of cover. However, this method has the advantage of giving the horizontal location of the pipeline's section limits, which is not the case with the 2D method.

Unlike the electromagnetic method, this method does not require injecting an alternating current in the pipeline. Moreover, SKIPPER NDT's mapping technology provides continuous data allowing to identify pipeline crossings and other ferromagnetic anomalies nearby. Data collection is also done using an Unmanned Aerial Vehicle.

VI. REFERENCES

[1] Costello, S.B., Chapman, D.N., Rogers, C.D.F., Metje, N., 2007. Underground asset location and condition assessment technologies. *Tunnelling and Underground Space Technology*, 22, 524–542. https://doi.org/10.1016/j.tust.2007.06.001

[2] Hao, T., Rogers, C.D.F., Metje, N., Chapman, D.N., Muggleton, J.M., Foo, K.Y., Wang, P., Pennock, S.R., Atkins, P.R., Swingler, S.G., Parker, J., Costello, S.B., Burrow, M.P.N., Anspach, J.H., Armitage, R.J., Cohn, A.G., Goddard, K., Lewin, P.L., Orlando, G., Redfern, M.A., Royal, A.C.D., Saul, A.J., 2012. Condition assessment of the buried utility service infrastructure. *Tunnelling and Underground Space Technology*, 28, 331–344. https://doi.org/10.1016/j.tust.2011.10.011

[3] Darilek, G.T.and Cooper Jr., E.H., 1985. Detecting buried pipeline depth and location with electromagnetic triangulation. Sep. 17, 1985, uS Patent 4,542,344.

[4] Olsson, M.S., Cox, D.A., Martin, M.J., Merewether, R., Jessup, A.H., 2012. System and method for locating buried pipes and cables with a man portable locator and a transmitter in a mesh network. Sep. 11, 2012, uS Patent 8,264.226 B1.

[5] Radiodetection, 2017. The theory of buried cable and pipe location. https://www.radiodetection.com/sites/default/files/Theory-Buried-pipe-manual-V10.pdf

[6] Fnaiech, E.A., Munschy, M., Corbineau, S., Marzin, M., Rohart, P., Takillah, S., 2020. Large stand-off magnetometry (LSM) for buried pipeline inspection., in: 15th Pipeline Technology Conference. Berlin, 12 pp.

[7] Vo, C.K., Staples, S.G.H., Cowell, D.M.J., Varcoe, B.T.H., Freear, S., 2020. Determining the Depth and Location of Buried Pipeline by Magnetometer Survey. *J. Pipeline Syst. Eng. Pract*, 11, 04020001-1. https://doi.org/10.1061/(ASCE)PS.1949-1204.0000438

[8] Li, C., Liu, D., Meng, J., Liu, J., Zhang, Y., 2020. The positioning of buried pipelines from magnetic data. *Geophysics*, 85, J111–J120.

[9] Leliak, P., 1961. Identification and Evaluation of Magnetic- Field Sources of Magnetic Airborne Detector EqllÎpped Aircraft. IEEE Transactions on aerospace and navigational electronics 8, 95–106.

[10] Leach, B.W., 1980. Aeromagnetic compensation as a linear regression problem. Information linkage between Applied Mathematics and Industry II, Academic Press, London 139–161.

[11] Olsen, N., Risbo, T., Brauer, P., Merayo, J., Primdahl, F., Sabaka, T., 2001. In-flight calibration methods used for the Oersted Mission. Ground and In-Flight Space Magnetometer Calibration Techniques, edited by A. Balogh and F. Primdahl, ESA SP-490, ESA Publishing Division, ESTEC, Katwijk, The Netherlands, 12.

[12] Munschy, M., Boulanger, D., Ulrich, P., Bouiflane, M., 2007. Magnetic mapping for the detection and characterization of UXO: Use of multi-sensor fluxgate 3-axis magnetometers and methods of interpretation. Journal of Applied Geophysics 61, 168–183. https://doi.org/10.1016/j.jappgeo.2006.06.004

[13] Nabighian, M. N., 1972. The analytic signal of two-dimensional magnetic bodies with polygonal cross-sections: Its properties and use for automated anomaly interpretation. GEOPHYSICS 37, 507–517. https://doi.org/10.1190/1.1440276

[14] Le Maire, P., Munschy, M., 2018. 2D potential theory using complex algebra: New equations and visualization for the interpretation of potential field data. GEOPHYSICS 83, J1–J13. https://doi.org/10.1190/geo2016-0611.1

[15] Nabighian, M.N., 1984. Toward a three-dimensional automatic interpretation of potential field data via generalized Hilbert transforms: Fundamental relations. GEOPHYSICS 49, 780–786. https://doi.org/10.1190/1.1441706

[16] Roest, W.R., Verhoett, J., Pilkington, M., 1992. Magnetic interpretation using the 3-D analytic signal. GEOPHYSICS 57, 116–125. https://doi.org/10.1190/1.1443174

[17] Salem, A., Ravat, D., Gamey, T.J., Ushijima, K., 2002. Analytic signal approach and its applicability in environmental magnetic investigations. Journal of Applied Geophysics 49, 231–244. https://doi.org/10.1016/S0926-9851(02)00125-8